Electronic Supplementary Material

**Partial acquisition of spectral projections accelerates four-dimensional spectral-spatial EPR imaging for mouse tumor models: A feasibility study**

Journal: Molecular Imaging and Biology

Misa Oba,[1] Mai Taguchi,[1] Yohei Kudo,[1] Koya Yamashita,[2] Hironobu Yasui,[3] Shingo Matsumoto,[4] Igor A. Kirilyuk,[5] Osamu Inanami,[3] Hiroshi Hirata[4*]

[1] Division of Bioengineering and Bioinformatics, Graduate School of Information Science and Technology, Hokkaido University, North 14, West 9, Kita-ku, Sapporo, 060-0814, Japan

[2] Laboratory of Radiation Biology, Graduate School of Veterinary Medicine, Hokkaido University, North 18, West 9, Kita-ku, Sapporo, 060-0818, Japan

[3] Laboratory of Radiation Biology, Faculty of Veterinary Medicine, Hokkaido University, North 18, West 9, Kita-ku, Sapporo, 060-0818, Japan

[4] Division of Bioengineering and Bioinformatics, Faculty of Information Science and Technology, Hokkaido University, North 14, West 9, Kita-ku, Sapporo, 060-0814, Japan

[5] N. N. Vorozhtsov Novosibirsk Institute of Organic Chemistry, 9, Ac. Lavrentieva Ave., Novosibirsk, 630090, Russia

* Corresponding author
Hiroshi Hirata, Ph.D.
E-mail: hhirata@ist.hokudai.ac.jp

Contents

**Supplementary Text S1**

A trick of accelerating the computation for Eq. (8) is briefly described here. The typical settings in our 4D spectral-spatial imaging were the number of voxels in 3D space $n = 72^3 =$ 373,248 and the number of data points in EPR spectra $m = 512$. So, $nm$ is equal to 191,102,976.

The product of ($nm \times m$) matrix $\boldsymbol{A}_j^{\mathrm{T}}$ and ($m \times m$) matrix $\boldsymbol{w}^{-1}$ is computationally expensive because the matrix $\boldsymbol{A}_j^{\mathrm{T}}$ is large. Moreover, since $\boldsymbol{A}_j^{\mathrm{T}}$ and $\boldsymbol{w}^{-1}$ have many zero elements, the product of these matrices is less efficient. To speed up the computation of Eq. (8), we replaced this computation with another approach in the computation code.

Here is Eq. (4) in the article:

$$\boldsymbol{s}_{4\mathrm{D},j+1} = \boldsymbol{s}_{4\mathrm{D},j} + \boldsymbol{A}_j^{\mathrm{T}} \boldsymbol{w}_j^{-1} \Delta \boldsymbol{f}_j \,. \quad (4)$$

Since the matrix $\boldsymbol{A}_j^{\mathrm{T}}$ is a back projection operator for the data of the difference $\Delta\boldsymbol{f}_j$ to the image matrix $\boldsymbol{s}_{4\mathrm{D},j}$, it is sufficient if the data of $\Delta\boldsymbol{f}_j$ are added to the image matrix with weight coefficients $\boldsymbol{w}_j^{-1}$. Under the magnetic field gradient $\boldsymbol{G}_j$, we defined ($n \times m$) array $\boldsymbol{M}_j$ containing the indexes of the image matrix $\boldsymbol{s}_{4\mathrm{D}}$, to which the elements of difference $\Delta\boldsymbol{f}_j$ are added. Instead of a large matrix product, we added the data of $\Delta\boldsymbol{f}_j$ with weight coefficients to the image matrix by sequentially reading the elements in array $\boldsymbol{M}_j$. For each magnetic field gradient setting, array $\boldsymbol{M}_j$ is updated.

## Supplementary Figure S1

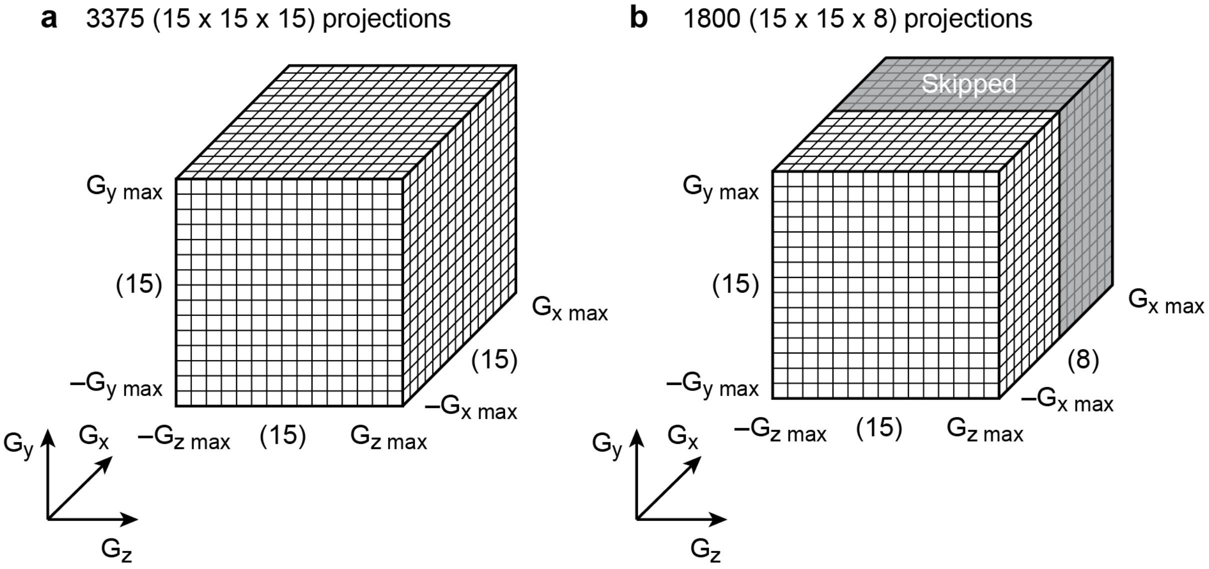


**Figure S1:** Raster magnetic field gradient (MFG) settings for (**a**) 3375 (15 × 15 × 15) projections and (**b**) 1800 (15 × 15 × 8) projections. In the MFG setting in panel **b**, the MFGs in the *x*-direction (the gray region) were initially skipped in the spectral projection data.

**Supplementary Figure S2**

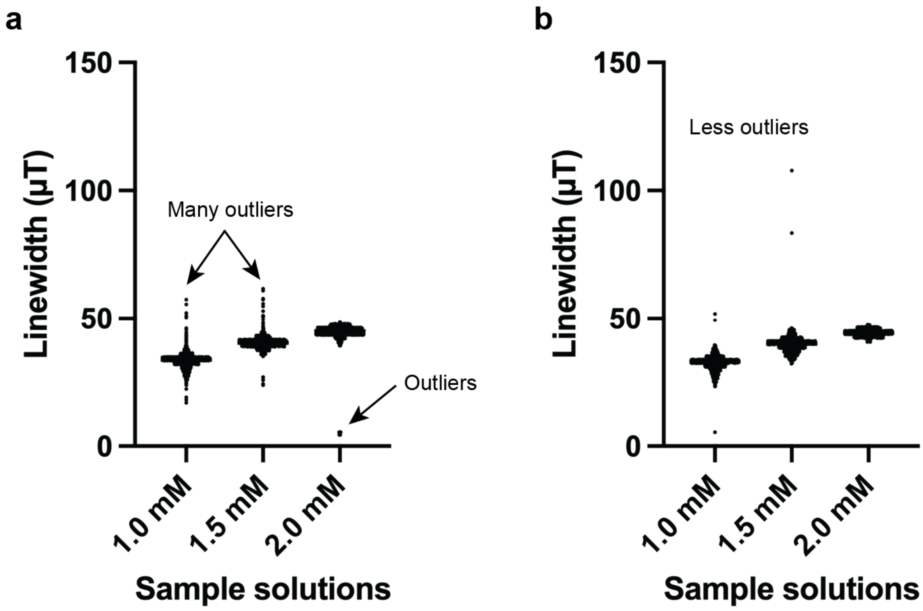


**Figure S2:** Individual value plots for the linewidth data. (**a**) The linewidths reconstructed from the data set of 1800 spectral projections, and (**b**) the linewidths reconstructed from the data set of 1800 spectral projections with spectral synthesis. These individual value plots depict the same linewidth data shown in Fig. 4g (middle and right panels). In panel **a**, there are many outliers, which are not visible in the middle panel of Fig. 4. In panel **b**, outliers are present but significantly less compared to panel **a**.

**Supplementary Table 1**
Summary of data acquisition strategies in studies on 4D spectral-spatial CW-EPR imaging.

| Articles on 4D spectral-spatial EPR imaging | Coordinates of magnetic field gradients | Magnetic field gradient settings | Image reconstruction |
|---|---|---|---|
| P. Kuppusamy *et al*., *J Magn Reson Ser B* **107**, 116–125 (1995) | Polar coordinates | Half sphere and sampling at equal linear angles | Convoluted back-projection |
| M. Elas *et al*., *Magn Reson Med* **49**, 682–691 (2003) | Polar coordinates | Half sphere and sampling at equal linear angles | 3-stage back-projection |
| M. Elas *et al*., *Clin Cancer Res* **12**, 4209–4217 (2006) | Polar coordinates | Half sphere and sampling at equal linear angles | 3-stage back-projection |
| K.-H. Ahn *et al*., *J Magn Reson* **185**, 152–158 (2007) | Polar coordinates | Half sphere and sampling at uniform solid angles | 3-stage back-projection |
| K.-H. Ahn *et al*., *J Magn Reson* **187**, 1–9 (2007) | Polar coordinates | Half sphere and sampling at uniform solid angles | Filtered back-projection |
| K.-H. Ahn *et al*., *Med Phys* **34**, 1047–1052 (2007) | Polar coordinates | Half sphere * | Filtered back-projection |
| R. Ahmad *et al*., *J Magn Reson* **187**, 277–287 (2007) | Polar coordinates | Full sphere and sampling at equal linear angles, equal solid angles, and uniform distribution defined by Feket points | Filtered back-projection |
| D. A. Komarov *et al*., *J Magn Reson* **281**, 44–50 (2017) | Orthogonal coordinates | Full space of 3D raster magnetic field gradient settings | Algebraic reconstruction technique |
| D. A. Komarov *et al*., *Anal Chem* **90**, 13938–13945 (2018) | Orthogonal coordinates | Full space of 3D raster magnetic field gradient settings | Algebraic reconstruction technique |
| A. Taguchi *et al*., *Analyst* **145**, 3236–3244 (2020) | Orthogonal coordinates | Full space of 3D raster magnetic field gradient settings | Algebraic reconstruction technique |
| Z. Zhang *et al*., *J Magn Reson* **350**, 107432 (2023) | Polar coordinates | Limited angular range in half sphere | Optimization problem with constraints |
| Z. Zhang *et al*., *J Magn Reson* **361**, 107654 (2024) | Polar coordinates | Sparse sampling in half-sphere | Optimization problem with constraints (TV and directional TV) |
| R. Nakaoka *et al*., *Anal Chem* **95**, 3940–3950 (2023) | Orthogonal coordinates | Full space of 3D raster magnetic field gradient settings | Algebraic reconstruction technique |
| **Present work** | Orthogonal coordinates | Full/partial space of 3D raster magnetic field gradient settings | Algebraic reconstruction technique |

* Note: There is no explicit description of sampling at uniform solid angles. However, field gradient direction settings might resemble their work (*J Magn Reson* **185**, 152–158, 2007).

**Supplementary Table S2**
Normalized root-mean-square error (NRMSE) for the linewidth maps reconstructed with various numbers of spectral projections under the 5% noise amplitude condition with the numerical phantom (Fig. 3a).

| Number of iterations | Number of spectral projections | | | | | | | |
|---|---|---|---|---|---|---|---|---|
| | 1800 | 2025 | 2250 | 2475 | 2700 | 2925 | 3150 | 3375 |
| 1 | 0.3159 | 0.1556 | 0.1502 | 0.1465 | 0.0767 | 0.0783 | 0.0782 | 0.0968 |
| 2 | 0.1859 | 0.0810 | 0.0776 | 0.0681 | 0.0543 | 0.0529 | 0.0530 | 0.0500 |
| 3 | 0.1135 | 0.0728 | 0.0695 | 0.0612 | 0.0511 | 0.0499 | 0.0496 | 0.0485 |
| 4 | 0.0844 | 0.0640 | 0.0618 | 0.0560 | 0.0496 | 0.0483 | 0.0482 | 0.0464 |
| 5 | 0.0753 | 0.0598 | 0.0580 | 0.0515 | 0.0482 | 0.0477 | 0.0476 | 0.0447 |
| 6 | 0.0666 | 0.0575 | 0.0561 | 0.0497 | 0.0476 | 0.0471 | 0.0470 | 0.0430 |
| 7 | 0.0613 | 0.0562 | 0.0546 | 0.0483 | 0.0471 | 0.0462 | 0.0466 | 0.0420 |
| 8 | 0.0583 | 0.0551 | 0.0532 | 0.0478 | 0.0462 | 0.0448 | 0.0453 | 0.0411 |
| 9 | 0.0542 | 0.0542 | 0.0518 | 0.0479 | 0.0451 | 0.0439 | 0.0444 | 0.0397 |
| 10 | 0.0520 | 0.0534 | 0.0513 | 0.0484 | 0.0442 | 0.0428 | 0.0434 | 0.0386 |
| 11 | 0.0506 | 0.0529 | 0.0507 | 0.0480 | 0.0436 | 0.0414 | 0.0418 | 0.0381 |
| 12 | 0.0490 | 0.0526 | 0.0504 | 0.0478 | 0.0425 | 0.0408 | 0.0407 | 0.0378 |
| 13 | 0.0482 | 0.0527 | 0.0500 | 0.0477 | 0.0414 | 0.0400 | 0.0404 | 0.0379 |
| 14 | 0.0478 | 0.0528 | 0.0500 | 0.0475 | 0.0410 | 0.0395 | 0.0396 | 0.0375 |
| 15 | 0.0477 | 0.0527 | 0.0501 | 0.0475 | 0.0405 | 0.0388 | 0.0388 | 0.0374 |
| 16 | 0.0473 | 0.0527 | 0.0498 | 0.0474 | 0.0400 | 0.0383 | 0.0383 | 0.0375 |
| 17 | 0.0461 | 0.0529 | 0.0498 | 0.0475 | 0.0396 | 0.0379 | 0.0377 | 0.0376 |
| 18 | 0.0453 | 0.0530 | 0.0496 | 0.0475 | 0.0392 | 0.0376 | 0.0375 | 0.0376 |
| 19 | 0.0447 | 0.0529 | 0.0495 | 0.0477 | 0.0388 | 0.0374 | 0.0374 | 0.0377 |
| 20 | 0.0437 | 0.0528 | 0.0494 | 0.0477 | 0.0386 | 0.0373 | 0.0373 | 0.0378 |
| 21 | 0.0433 | 0.0527 | 0.0495 | 0.0476 | 0.0381 | 0.0373 | 0.0371 | 0.0377 |
| 22 | 0.0429 | 0.0525 | 0.0495 | 0.0475 | 0.0379 | 0.0373 | 0.0372 | 0.0378 |
| 23 | 0.0428 | 0.0524 | 0.0495 | 0.0475 | 0.0379 | 0.0373 | 0.0372 | 0.0378 |
| 24 | 0.0426 | 0.0523 | 0.0494 | 0.0476 | 0.0377 | 0.0375 | 0.0374 | 0.0378 |
| 25 | 0.0424 | 0.0522 | 0.0494 | 0.0474 | 0.0375 | 0.0374 | 0.0375 | 0.0378 |
| 26 | 0.0423 | 0.0522 | 0.0494 | 0.0474 | 0.0376 | 0.0374 | 0.0375 | 0.0378 |
| 27 | 0.0423 | 0.0522 | 0.0494 | 0.0475 | 0.0375 | 0.0374 | 0.0375 | 0.0378 |
| 28 | 0.0424 | 0.0521 | 0.0494 | 0.0474 | 0.0375 | 0.0373 | 0.0374 | 0.0378 |
| 29 | 0.0424 | 0.0521 | 0.0494 | 0.0473 | 0.0375 | 0.0373 | 0.0375 | 0.0377 |
| 30 | 0.0421 | 0.0521 | 0.0494 | 0.0473 | 0.0375 | 0.0374 | 0.0375 | 0.0377 |